Electrically Excited, Supersonic Flow Carbon Monoxide Laser

J. W. RICH,* R. C. BERGMAN,† AND J. A. LORDI‡
Calspan Corporation, Buffalo, N.Y.

A study of CW electric-discharge-excited supersonic flow carbon monoxide lasers is presented. Recent experimental results are reported for a device utilizing a high-pressure glow discharge in the plenum of a supersonic nozzle. An optical cavity is established transverse to the supersonic flow at an effective nozzle area ratio of $A/A^* = 8.9$. CW powers in excess of 300 watts and efficiencies of 10% are obtained. More than 60% of the output power is at wavelengths below 5.10 μ. The experimental data are compared with the predictions of a computer model of the laser performance.

I. Introduction

THE direct-discharge-excited carbon monoxide laser has demonstrated the remarkable efficiency of a glow discharge for exciting the vibrational quantum states of CO.[1-3] Continuous wave operation of carbon monoxide lasers has been achieved in which nearly 50% of the input electrical power is converted into laser output on the fundamental vibration-rotation bands.[4] This efficiency is the highest reported for any cw laser, and makes the CO laser an attractive candidate for many IR applications. There are, however, some significant problems associated with the use of powerful CO lasers. Of direct concern to the present work is that the output wavelengths of conventional CO lasers operating at peak efficiency are from 5.1 to 5.6 μ. This output corresponds to vibrational bands $V = 6 \rightarrow 5$ to $V = 17 \rightarrow 16$. Unfortunately, part of the v_2 bands of water vapor also occur in this wavelength range. Many of the most powerful CO laser spectral lines are significantly attenuated during transmission through the atmosphere, due to absorption by the wing of R-branch $v_0 \rightarrow v_2$ transitions in H_2O. A second problem is that the techniques used to maximize efficiency are costly, and are not necessarily scalable to large devices. Specifically, conventional CO lasers use discharge tubes cooled by static wall baths. Peak efficiency is reported with liquid N_2 cooling; efficiency is reduced by 90% under room temperature operating conditions. Secondly, at both room temperature and cryogenic temperature conditions, xenon is used as a gas additive; operation without Xe also greatly reduces efficiency.

The present paper discusses the performance of an electrically excited carbon monoxide laser which utilizes gas dynamic cooling. This laser was designed to eliminate the problems discussed in the preceding paragraph. A preliminary report of the laser was published at an early stage of development.[5]

The use of gas dynamic cooling in a CO laser was motivated by theoretical studies[6-10] of vibrational energy exchange processes in CO laser gas environments. These studies suggested that high output power from vibrational bands below $V = 6 \rightarrow 5$ could be obtained, if the gas translational temperature were lower than that obtainable in statically cooled discharge tubes. Laser output on bands below $V = 6 \rightarrow 5$ in CO corresponds to wavelengths below 5.1 μ; such wavelengths can be more suitable for atmospheric transmission, as they are less overlapped by water vapor absorption bands. This prediction of shorter wavelength output with decreasing temperature has been verified by experiments in shock tunnels.[11-12] In these experiments, high-temperature mixtures of CO and Ar, created behind a reflected shock in a shock tube, were expanded in a supersonic nozzle. Optical cavities, established transverse to the flow at large expansion area ratios ($A/A_{throat} > 500$), create powerful cw laser action for the duration of the steady flow. McKenzie[11] has shown that more than 50% of the output from such a system can be from wavelengths below 5.0 μ, i.e., from vibrational levels $V = 5$ and below. It should be noted, however, that thermal excitation of the laser gases is a relatively inefficient means of energizing the vibrational mode of CO. At the 2000 K plenum conditions of the shock-tunnel-driven CO gas-dynamic lasers, only about 20% of the equilibrium thermal energy is in the vibrational mode. This percentage represents an inherent upper limit on the maximum efficiency of a thermally excited CO gas-dynamic laser. Such a system cannot, therefore, attain the efficiency already achieved in discharge-excited CO lasers. For this reason, the laser discussed in the present paper uses an electric discharge to energize the CO vibrational mode.

The following sections report the results of experimental and analytical studies in the electrically excited supersonic flow CO laser. Section II describes the laser, and presents results of performance and diagnostic experiments in the device. Section III summarizes theoretical models and numerical codes used to analyze the laser performance, and gives a comparison with experimental results. A summary and some conclusions are given in Section IV.

II. Experimental Studies

Laser Geometry

Figure 1 shows a perspective schematic sketch of the electrically excited gas dynamic carbon monoxide laser. Figure 2

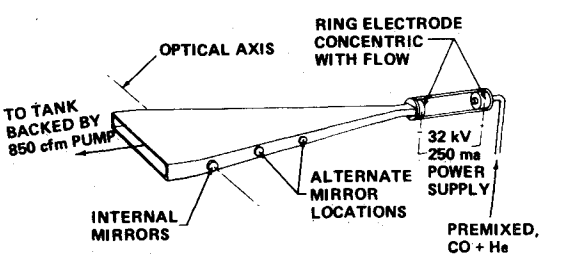

Fig. 1 Perspective sketch of the electrically excited supersonic flow CO laser.

Presented as Paper 74-179 at the AIAA 12th Aerospace Sciences Meeting, Washington, D.C., January 30–February 1, 1974; submitted April 5, 1974; revision received August 2, 1974. This research was supported by the United States Air Force Avionics Laboratory under Contract F33615-73-C-1285 and United States Army Missile Command and Advanced Research Projects Agency, Contract DAAH01-72-C-0936 under ARPA Order 1180. The authors gratefully acknowledge the assistance of E. Simme in the conduct of the experiments and the assistance of J. Moselle in the programing of the numerical code used.

Index categories: Lasers; Atomic, Molecular, and Plasma Properties.

* Principal Engineer, Aerodynamic Research Department.

† Assistant Physicist, Aerodynamic Research Department.

‡ Principal Engineer, Aerodynamic Research Department. Member AIAA.

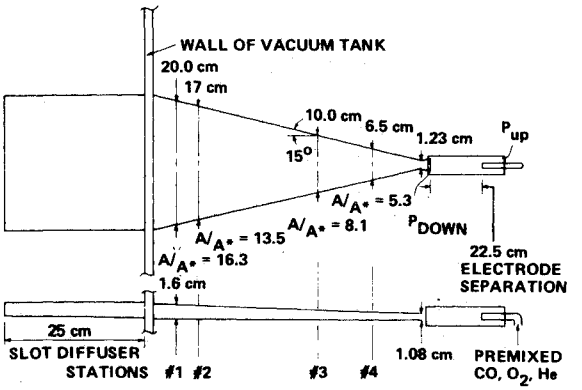

Fig. 2 Schematic diagram of the electrically-excited supersonic flow CO laser.

gives the critical dimensions of the laser. The laser uses a direct current electrical discharge to excite a mixture of CO and He; subsequent to excitation, the gas mixture is cooled by a supersonic gas dynamic expansion. Referring to Figs. 1 and 2, the discharge tube consists of a $1\frac{1}{2}$ in. i.d. pyrex pipe, which forms the plenum chamber of the supersonic nozzle. The anode is a water-cooled hollow brass and copper pipe which also functions as a gas-dynamically choked orifice through which the premixed gases are injected into the discharge tube. Details of the anode design are discussed in the following section. The cathode is formed by the nozzle throat itself, which is a water-cooled brass section, with throat dimensions of 1.2 × 1.1 cm. The nozzle is of rectangular cross section, as shown. The expansion half-angle is 15°, and the top and bottom surfaces diverge slightly to allow for boundary-layer growth. The system currently is being pumped by the Calspan flow laser facility, which consists of a 125,000 cu ft vacuum sphere backed by 850 cfm vacuum pumps. Use of this facility to pump the laser permits essentially continuous supersonic operation.

Discharge Operating Characteristics

The laser has been operated at discharge pressures from less than 0.5 atm to 1.5 atm. Operating pressures in this range are obtainable only with a large preponderance of helium diluent. Reduction of the amount of helium diluent creates discharge instabilities which very rapidly result in arc breakdown of the discharge. The use of diluents other than helium gave unsatisfactory results; the maximum discharge pressures obtainable were quite low, and laser performance was in no way comparable to those achieved with helium. The role of helium in increasing discharge stability is, apparently, to insure rapid dissipation of local arc filament "hot spots" by increasing the heat conductivity of the discharge gases. Such heat dissipation prevents growth of arc filaments and subsequent arc breakdown of the discharge. It should be noted that, unlike CO_2 gas dynamic lasers, helium plays no critical role in enhancing pumping of the population inversion. Indeed, helium, as a fast vibration-to-translation (V-T) relaxer, potentially can degrade the population inversions in a CO laser. Secondly, unlike conventional wall-cooled CO lasers, helium is not required to insure rapid thermal transport to cold walls. The validity of these two points is demonstrated by the operation of the thermally excited CO gas dynamic lasers previously mentioned.[11-12] These systems, not using an electric discharge, do not require the stabilizing effect of helium, and perform quite well with either argon or nitrogen diluents.

Most of the data presented in this paper were obtained at a discharge pressure of 350 torr. At this pressure, the upstream electrode (the anode) consisted of a $\frac{1}{2}$ in. i.d. pipe, through which gases were injected at sonic velocity parallel to the discharge axis. Recently, however, stable discharge operation has been achieved at supra-atmospheric pressures (to 1.5 atm) using an annular slot injector anode similar to that developed by Gibbs and McLeary.[13] In this configuration, the anode is in the form of a 1 in. i.d. pipe, which contains a circumferential slot through which gases are injected normally to the discharge axis. The slot width is just sufficient to choke the gas flow. This method of gas injection creates a radial flow velocity component in the vicinity of the anode. As discussed in detail in Ref. 13, this velocity component promotes the rapid dissipation of incipient streamwise arc filaments, and thereby increases discharge stability.

The power supplies used for the laser are Universal Voltronics d.c. voltage regulated supplies, equipped with saturable core reactor current limiting circuits. With the current limiter, it is possible to prevent large current surges which precede total arc breakdown of the discharge. Operation with the current limiter significantly extends the stable operating region of the discharge, permitting operation at currents into the arc transition region. It should be noted that series ballast resistance is minimal in the present setup, amounting to less than 1% of the discharge impedance. During normal operation, the milky-blue glow of the positive column of the CO/He discharge fills the discharge tube with a fairly uniform intensity.

Gas Dynamic Performance

The principal gas dynamic diagnostic in the laser is the measurement of wall static pressure. There are pressure measurement taps at each station indicated in Fig. 2. These taps are located in the bottom wall of the nozzle close to the centerline. Pressures are measured with an MKS Industries "Baratron" gage. Static pressure in the discharge section can also be measured at both the upstream and downstream ends of the discharge tube, as indicated in Fig. 2. Under the present operating conditions of the laser, the upstream and downstream discharge pressure measurements are essentially equal; the flow velocity in the discharge tube is sufficiently slow that the discharge static pressure measurement can be taken as equal to the stagnation pressure.

Figure 3 shows the static pressure distribution down the nozzle for the typical operating conditions indicated on the graph. Also shown are the Mach number variation, as calculated from the pressure measurements, and a comparison with the pressure and Mach number distribution predicted for an ideal isentropic nozzle. From these data, it can be seen that the laser shows considerable departure from the isentropic nozzle prediction at higher expansion ratios. This departure can be attributed to two causes: 1) boundary-layer growth, which is particularly marked at the low density, high expansion portion of the nozzle, and 2) the highly nonequilibrium kinetic processes occurring in the gas flow, specifically, the influence of nonequilibrium vibrational processes. However, boundary-layer growth is the dominant

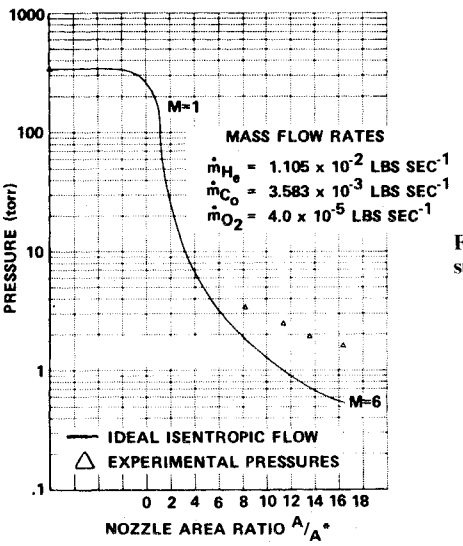

Fig. 3 Static pressure distribution in the laser.

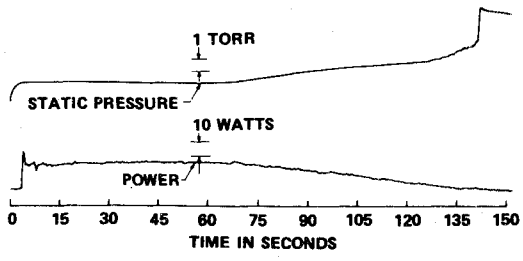

Fig. 4 Power and pressure histories during a single run period.

influence in the present case. Estimates of boundary-layer displacement thickness in the nozzle predict a departure from the inviscid expansion theory of very nearly the same size as that observed.

The supersonic flow pattern as given in Fig. 3 will remain steady as long as the pressure at the nozzle exit does not become too large. However, when the pressure in the vacuum sphere rises to several times the nozzle static pressure at the farthest downstream station (No. 1), a shock pattern moves up the nozzle, destroying the supersonic flow. This phenomenon is shown in Fig. 4, in which static pressure and laser power at nozzle Station No. 1 are plotted as functions of time.§ These data show that supersonic flow is definitely required to sustain laser operation in the present configuration. It can be noted from Fig. 6 that, after flow initiation at $t = 0$, the static pressure in the cavity quickly rises to a steady "plateau" of approximately 1.5 torr. After discharge initiation (at $t \approx 4$ sec), laser power also is established at a steady value of approximately 15 w. At approximately 65 sec, static pressure in the cavity begins to rise. This rise in static pressure is due to a flow separation phenomenon. Back pressure at the nozzle exit has risen to a value such that the flow is separating from the regions near the nozzle walls, and a separation shock system begins to move through the laser cavity. It can be observed that laser power now begins to fall off. Pressure continues to rise until all supersonic flow ends at approximately $t = 135$ sec, and laser output ceases entirely.

Optics

The optical cavity in the laser was established using a mirror system consisting of a 4 m radius of curvature total reflector

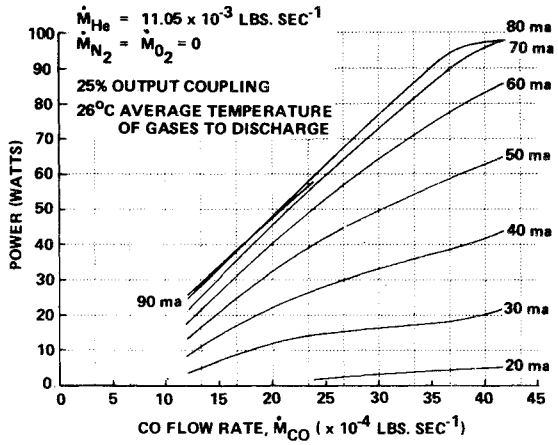

Fig. 5 Power vs CO flow-rate, room temperature operation.

§ The data of Fig. 4 were deliberately selected to illustrate a limited-pumping-capacity case, in which back pressure quickly rose to a value sufficient to create separation. The run times and the laser power given in Fig. 6 are not typical of the current performance levels of the system.

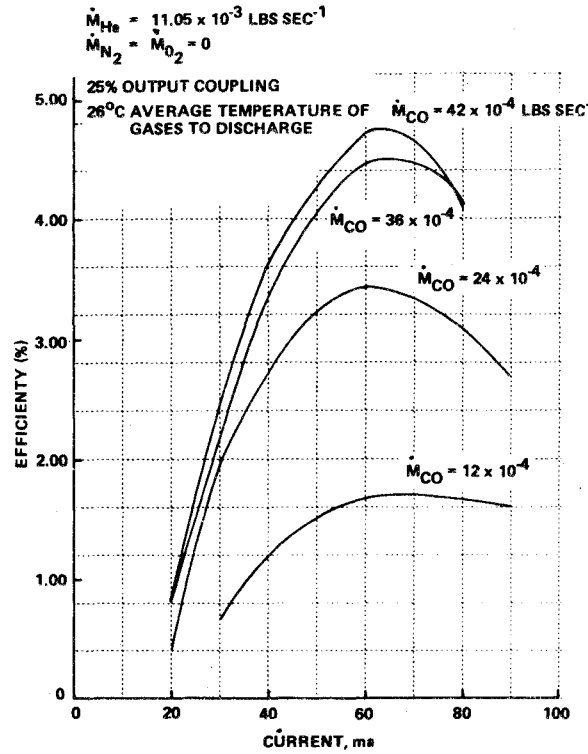

Fig. 6 Efficiency vs current, room temperature operation.

and a dielectric-coated germanium flat. The mirrors were obtained commercially. The mirrors are internally mounted, in cylindrical mirror boxes which can be bolted in place at any of the nozzle stations shown in Fig. 2. The laser data reported in this paper were all obtained with an optical cavity at the farthest downstream location in the nozzle, Station No. 1 in Fig. 2.

Laser Performance

Figures 5 and 6 illustrate the laser performance at the 350 torr discharge level. These data were obtained with the straight axial flow injector anode. Figure 5 is a plot of the laser power vs the CO flow rate. Results are shown for various discharge currents in the range 20 to 90 ma. It can be seen that laser power increases monotonically with CO flow rate for all values of the discharge current. Above 80–90 ma, the discharge arced, and data were unobtainable. It should also be noted that at the higher CO flow rates, power reaches a maximum at currents of approximately 70–80 ma; operation at currents above this range did not increase output power. Finally, at CO flow rates above the maximum shown (4.2×10^{-3} lbs/sec), the discharge became quite unstable; continuous glow discharge operation was not possible. At the maximum CO flow rate of 4.2×10^{-3} lbs/sec, CO comprised 5% by volume of the gas in the discharge; the remainder of the mixture was helium. If the fraction of CO in the mixture is raised much above 5%, the thermal conductivity of the gas mixture becomes significantly reduced. It is this reduction of thermal conductivity that probably causes the onset of arc instabilities with increasing CO concentration. At high CO concentrations, heat dissipation from incipient arc filaments is reduced; increasing temperature in these filaments causes a reduction in the local gas number density. The increased local E/N ratio causes increased ionization in the filament, resulting in increased local current and filament growth, and leads to arc breakdown.

Operation of the discharge at currents above approximately 65 ma caused a decrease in efficiency, although laser power increased in some cases. This is illustrated in Fig. 6, in which efficiency is plotted against discharge current, for several

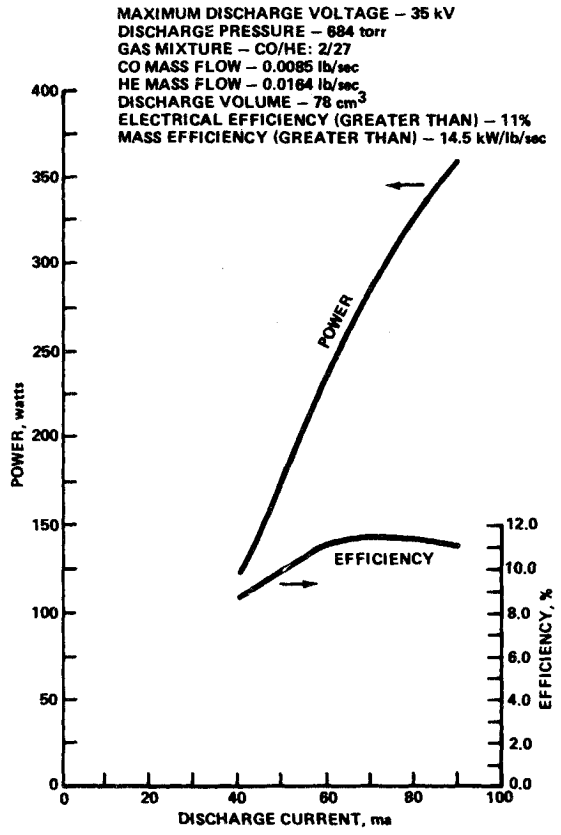

Fig. 7 CO supersonic laser performance at high discharge pressure.

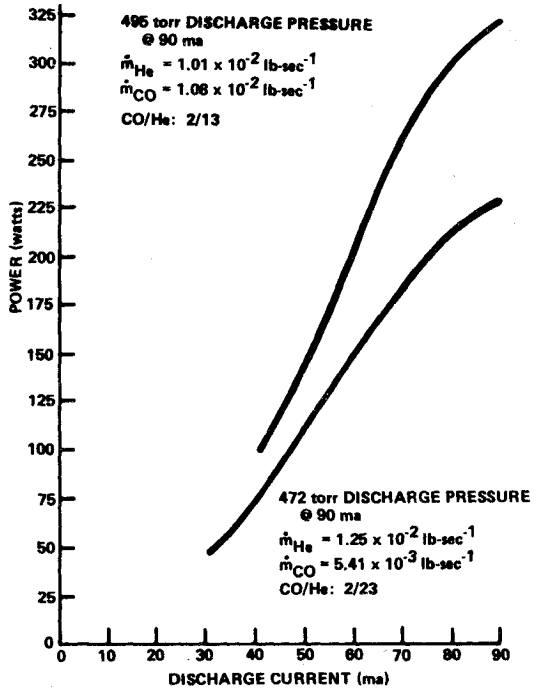

Fig. 8 CO supersonic laser performance at high CO concentration.

values of the CO flow rate. Efficiency is defined as the percent of electrical input power recovered as laser output radiation. Figure 6 also shows a continuous increase in efficiency with CO flow rate, for almost all values of discharge current.

Figures 7 and 8 illustrate the laser performance at higher discharge pressures, which were achieved using the annular slot injector anode of Ref. 13. Figure 7 plots laser power and efficiency vs discharge current, for a discharge pressure of 685 torr. The gases are entering the discharge at room temperature. The gas mass-flow rates and volumetric concentrations are indicated on the figure. Maximum power achieved was 360 w at 11% efficiency. Figure 8 shows results of a preliminary effort to assess the effect of increased CO concentration. To strike the discharge at higher CO concentrations, it was necessary to operate at the lower total pressure of 495 torr. The discharge was stable with CO concentration up to 15% and power increased with CO concentration.

Finally, Table 1 presents some preliminary results of operation of the laser at supra-atmospheric discharge pressures. Three cases are shown, all for discharge pressures of 1.5 atm. Stable discharge operation was obtained, but the percentage of CO was relatively small, being less than 4%. Accordingly, the mass efficiency (kw/lb/sec) is lower than for operation below 1 atm.

In Run Nos. 1 and 2 of Table 1, room temperature inlet gases were used. CO concentration was increased from 1.99% in Run 1 to 3.26% in Run 2, reaching a maximum mass efficiency of 9.17 kw/lb/sec and an electrical efficiency of 10.4%. In Run No. 3, gases precooled to 200°K were used, with a consequent increase in electrical efficiency to 11%. However, mass efficiency is somewhat less than the highest achieved with room temperature operation. It should be noted that pressures above 1.5 atm are not presently attainable due to limits of the gas handling system for the laser; this pressure does not represent a stability limit.

Figure 9 gives typical output spectra of the laser. Spectra are shown for output mirrors of four reflectivities, as indicated on the figure. The rotational and vibrational quantum numbers of the transitions are also given. The system lases on the vibrational bands from $V = 3 \rightarrow 2$ to bands above $V = 15 \rightarrow 14$. The most powerful lasing is on the lower vibrational quantum number bands, $V = 3 \rightarrow 2$ to $V = 7 \rightarrow 6$. These bands possess the shortest wavelengths of the output spectrum. Typically, more than 60% of the laser output is on lines of wavelengths below 5.1 μ. It should also be noted that the lines that are lasing have very low rotational quantum numbers, transitions as low as $J = 2 \rightarrow 3$ being observed. This behavior is in marked contrast to a conventional liquid nitrogen cooled CO laser, which produces almost all of its output above 5.1 μ, and which lases on higher rotational lines.

The most power was extracted from the laser with 85% reflectivity mirrors; however, as shown in Fig. 9, the system continued to lase even with a 55% reflecting mirror, at approximately 10% of the power obtained at 85% reflectivity. This is testimony

Table 1 High pressure operation of the electrically excited supersonic flow carbon monoxide laser

Run no.	Plenum pressure, atm	Inlet gas temperature, K	Mass flow of He, lb/sec^{-1}	Mass flow of CO, lb/sec^{-1}	Mole fraction of CO, %	Laser power, watts	Mass efficiency, kW/lb/sec	Electrical efficiency, %	Discharge voltage, kV	Discharge current, mA
1	1.5	300	0.0317	0.0045	1.99	290	8.01	9.1	40	80
2	1.5	300	0.0308	0.0073	3.26	350	9.17	10.4	48	70
3	1.5	200	0.0312	0.0055	2.44	300	8.17	11.0	44	62

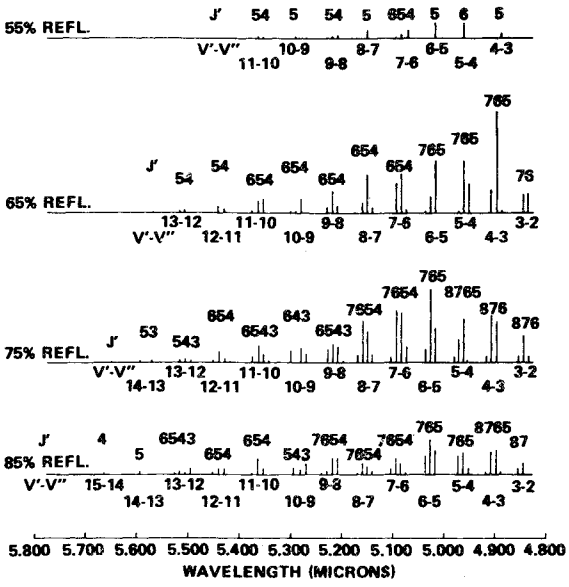

Fig. 9 CO laser spectra at various output couplings, room temperature operation.

to the high gain of the supersonic flow laser medium; the small signal gain is in excess of 1.5% per centimeter.

Rotational Temperature Measurement

The operating characteristics discussed above, most notably, the very low rotational quantum numbers of the lasing spectral lines, and the evident very high gain of the optical cavity, indicate that the supersonic expansion produces very low in-cavity translational/rotational temperatures. This is confirmed by a direct measurement of rotational temperature in the nozzle. This measurement was made by monitoring the spontaneous radiation emitted from the nozzle by the infrared fundamental vibrational-rotational bands of the CO. For this purpose, CaF_2 windows were installed at nozzle Stations 1, 3 and 4 in the laser (cf. Fig. 2). The windows were carefully designed to preserve a completely flush surface in the nozzle walls.

Most spontaneous radiation measurements were performed at Station No. 3 in the nozzle, with the optical path across the long dimension of the expansion. As can be seen from Fig. 2, the optical path at this station is 10 cm long. A schematic of the optical setup is shown in Fig. 10. As indicated in the figure, a mirror could be used on the far side of the nozzle from the spectrometer, to reflect emitted radiation back through the test section into the spectrometer. As discussed below, this double pass configuration could be used to measure the integrated absorption coefficients of individual rotational-vibrational lines in the spectrum. Radiation emitted through the window is collected and dispersed by a $\frac{1}{2}$ m Czerny-Turner scanning monochromator, equipped with a 300 line/mm, 4.00 μ blaze, Bausch and Lomb grating. Infrared output was detected by a Davers-type A-10, liquid-nitrogen-cooled InSb detector. The infrared signal was typically chopped at 800 Hz, using a Princeton Applied Research Model 191 mechanical chopper and synchronous motor; the detector output was amplified using a PAR Model 124 phase lock amplifier. The output spectra were recorded on a Varian chart recorder. The relative response of the instrument train, as a function of wavelength, was determined by scanning, at several temperatures, an Infrared Industries Model 464/1018 calibrated blackbody source.

Figure 11 shows a resolved spectrum giving the individual rotational lines of the R-branch of the $V = 1 \rightarrow 0$ band component. As discussed in standard references[14,15] if $I(J)$ is the peak intensity of the Jth rotational line, a plot of $\ln(I\lambda^4/J')$ vs $J'(J'+1)$ should be linear for an optically thin radiating gas.¶ Here, λ is the wavelength of the rotational line and J' is the rotational quantum number of the upper level in the transition. The slope of such a plot is equal to $B_e hc/kT_{ROT}$, where B_e is the rotational constant of the molecule ($=1.93$ cm^{-1} for CO), h, c, k are, respectively, Planck's constant, the speed of light, and Boltzmann's constant, and T_{ROT} is the rotational temperature. Hence, the rotational temperature can be determined directly from such a plot.

In the present experiment, the rotational line spectra were obtained using a horizontal optical path along the long dimension of the nozzle at Station No. 3. Further, a mirror was used on the far side of the nozzle from the spectrometer, as shown in Fig. 10. The long optical path was chosen to give adequate intensity to permit resolution of the individual rotational lines. If the gas were optically thin, the use of the reflecting mirror would double the signal received by the spectrometer, neglecting the mirror reflectivity and window transmission losses. However, under the present conditions, the gas is self-absorbing, and considerably less than double the single pass intensity is obtained when the return mirror is used. Assuming the gas conditions are homogeneous across the nozzle, it can be shown[16] that the intensity received at the spectrometer compared to the intensity that would be received for a single

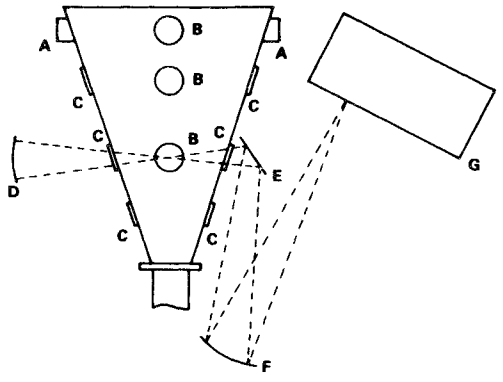

A – LASER CAVITY MIRROR MOUNTS
B – VERTICAL VIEWING CALCIUM FLUORIDE WINDOWS
C – HORIZONTAL VIEWING CALCIUM FLUORIDE WINDOWS
D – SPHERICAL MIRROR
E – ELLIPTICAL DIAGONAL MIRROR
F – SPHERICAL MIRROR
G – ½ METER GRATING MONOCHROMATOR

Fig. 10 Infrared sidelight experiment schematic.

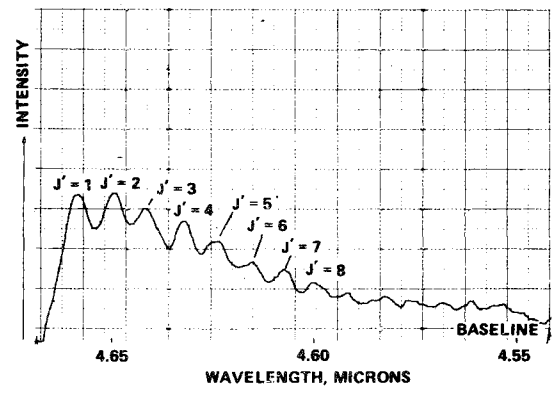

Fig. 11 Sidelight emission spectrum—resolution of rotational lines.

¶ The intensity must be corrected for any variation of the response of the instrumentation as a function of wavelength.

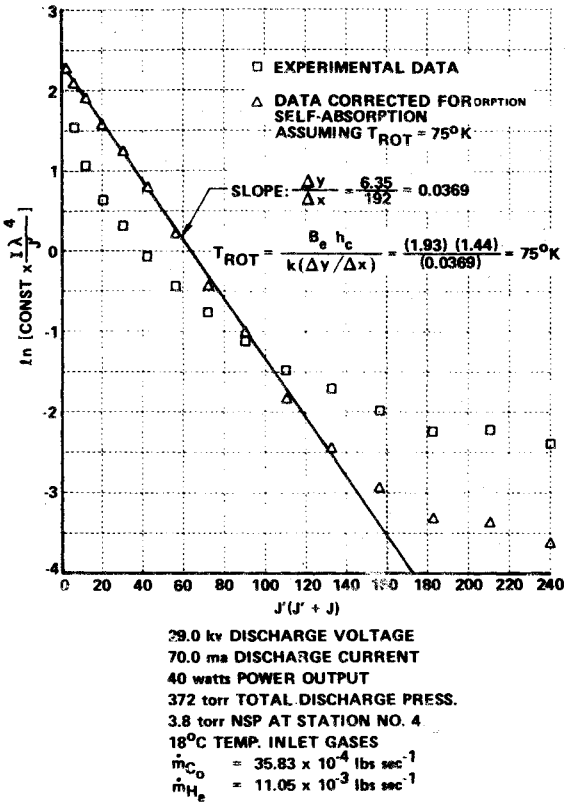

Fig. 12 Determination of rotational temperature.

pass, optically thin emitter is related to the absorption coefficient by:

$$\frac{I\text{ (Double pass, self-absorbing)}}{I\text{ (Single pass, optically thin)}} = \left\{\sum_{n=0}^{\infty} \frac{(1-P'x)^n}{(n+1)!\,(n+1)^{1/2}}\right\}\{1-\eta_W{}^2\eta_M\} + \left\{\sum_{n=0}^{\infty} \frac{(-2P'x)^n}{(n+1)!\,(n+1)^{1/2}}\right\}\{2\eta_W{}^2\eta_W\} \quad (1)$$

Here, P' is the absorption coefficient, in cm^{-1}, and x is the optical path length in cm. η_W is the transmission of the windows, and η_M is the mirror reflectivity. Note for $\eta_W = \eta_M = 1$, $P'x \to 0$, this ratio goes to 2.

Figure 12 shows a plot for determination of rotational temperature at Station No. 3 in the nozzle. The mass flow rates and discharge operating conditions are indicated on the figure. $\ln[\text{const} \times (I\lambda^4/J')]$ is plotted vs $J'(J+1)$, both with and without the intensity corrected according to Eq. (1). The self-absorption correction is applied in an iterative fashion. The rotational temperature is estimated, and the absorption correction calculated from Eq. (1). A new rotational temperature is then inferred from the slope of the corrected points. The iteration is ended when the estimated and inferred temperatures agree within 10%. The procedure is relatively insensitive to the ratio of the populations of the $V = 1$ and $V = 0$ vibrational states. The rotational temperature obtained from the slope of the corrected points is 75 K.

III. Theoretical Modeling of Laser Operation

There has been extensive theoretical modeling of kinetic processes in electrically excited CO lasers in the last few years. As part of the present investigation of electrically excited supersonic flow CO lasers, theoretical models and computer codes have been developed to predict performance. A detailed description of these modeling studies is given in Ref. 17. As the codes are applied to calculations of the present laser, the following operating conditions must be specified: 1) The mass flow rates of each constituent in the laser; 2) The inlet temperature of the gases; 3) The operating pressure in the discharge; 4) The cross-sectional area of the discharge tube, and the electrode separation in the discharge; 5) The operating voltage and current in the discharge; 6) The throat area and the expansion angle of the supersonic nozzle; 7) The location and streamwise extent of the optical cavity; 8) The mirror reflectivities and losses in the optical cavity.

Given these inputs, the following calculations are performed:

a) A Fokker-Planck type equation governing the electron energy distribution in the discharge is solved. The methods are similar to those published by Nighan.[2] Electron drift velocity, electron number density, and the rate of vibrational excitation of CO molecules by electron impact are calculated.

b) Equations governing the gas dynamic variables of pressure, temperature, and velocity, together with kinetic equations governing the populations of the individual CO vibrational quantum states, are solved simultaneously for these variables as functions of streamwise position.

c) Output power from the flow laser is calculated using a Fabry-Perot cavity (flat-flat mirrors) model, having an optical axis perpendicular to the flow direction. With this approximation, a quasi-one-dimensional flow calculation for the gas-dynamics and CO kinetics provides a consistent description of the coupling between these processes and the radiation field. A solution to this problem has all the essential coupling features but not the complexity of a curved mirror system. For this cavity model, the calculation of the gas-dynamic properties, vibrational level populations, and lasing intensities in a CO flow laser is like that used for chemical lasers by Emanuel.[19]

The equations that are solved are one-dimensional; distance in the flow direction is the only independent variable; variation of medium properties normal to the flow direction is neglected. The kinetic processes controlling the CO vibrational state populations included in the model are collisionally induced exchange of energy between the modes of CO vibration and heavy species translational and rotational motion; exchange between vibration and electron motion; vibration-to-vibration energy exchange among colliding CO molecules; and spontaneous radiative decay. References 6–10, 17 and 18 discuss the influence of these kinetic processes in detail.

Figures 13 and 14 show the calculated results for typical room temperature operation of the electrically excited supersonic flow laser. In Fig. 13, the variation of temperature, pressure, and vibrational energy through the laser is plotted. The operating conditions are as indicated on the figure. The gradual rise in power in the vibrational mode of the CO, as the gas is processed by the discharge, can be observed. An increase in translational temperature is also observed. These calculations indicate approximately 25% of the total electrical power goes into the CO vibrational mode. Very little of this vibrational mode power is lost as the gas is expanded in the nozzle. Typical measured temperature and pressures in the nozzle expansion are

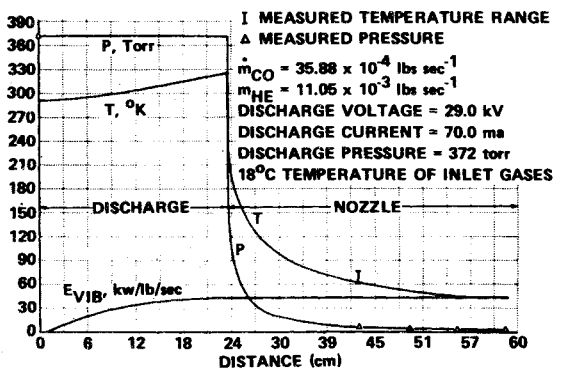

Fig. 13 Predicted pressure, temperature, and vibrational energy in the prototype CO supersonic flow laser.

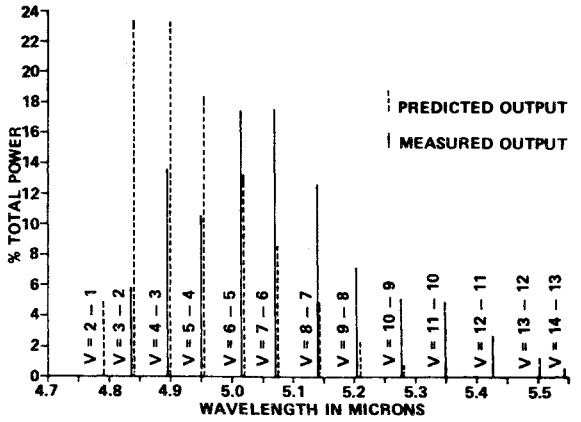

Fig. 14 Comparison of predicted and measured output in the prototype CO supersonic laser.

also shown. It should be noted that the expansion ratio of the nozzle in the calculated results was chosen to match the observed pressure distribution, i.e., the calculation is for the effective expansion ratio of the nozzle, not for the geometrical expansion.

On the basis of the preceding correlation of the theoretical model with measurements, a temperature of 40 K in the optical cavity at Station No. 1 (Fig. 2) is inferred. Figure 14 shows the spectral power distribution for the optical cavity at Station No. 1 ($A/A_{throat} = 8.9$) compared with the experimentally measured laser spectrum. It is seen that the spectral distributions are in approximate agreement; the theoretically predicted spectra show somewhat greater weighting of intensities at short wavelengths. This shift can perhaps be attributed to the experimental cavity being slightly warmer than the theoretically predicted 40 K. However, it is noteworthy that the peak gain rotational lines predicted coincide with those measured; these are the P(3) to P(6) lines in each band.

IV. Conclusions

The present electrically excited supersonic flow CO laser has been operated at power levels of ~350 w cw., at 12% efficiency and specific powers of 14.5 kw/lb/sec. For these operating conditions, the discharge pressure is 684 torr, and the in-cavity pressure is 2.5 torr. A correlation of theoretical calculation with measurements of rotational temperature in the nozzle expansion indicate an in-cavity temperature of 40 K. More than 60% of the output power is distributed among approximately 15 lines at wavelengths from 4.819–5.084 μ; the remaining power occurs on lines from 5.132 μ to above 5.758 μ.

Some principal findings of the present study are: 1) It is possible to operate a stable axial flow glow discharge in a CO/He plasma at pressures of at least 1.5 atm. 2) Use of electrical excitation and supersonic flow to obtain low in-cavity temperatures results in a powerful and efficient CO laser producing more than 60% of its output at wavelengths below 5.1 μ. 3) Lasing action has been obtained on many vibrational-rotational spectrum lines of CO with extremely low J values; these have not previously been identified in CO laser emission.

References

[1] Osgood, R. M., Jr., Eppers, W. C., Jr., and Nichols, E. R., "An Investigation of the High-Power CO Laser," *IEEE Journal of Quantum Electronics*, Vol. QE-6, No. 3, March 1970, pp. 145–154.

[2] Nighan, W. L., "Electron Kinetic Processes in CO Lasers," *Applied Physics Letters*, Vol. 20, No. 2, Jan. 1972, pp. 96–99.

[3] Rich, J. W., Watt, W. S., and Thompson, H. M., "Experimental and Theoretical Investigation of the Directly Excited Carbon Monoxide Laser; Final Technical Report," AFAL-TR-71-152, March 1971, U.S. Air Force Avionics Lab., Wright-Patterson Air Force Base, Ohio.

[4] Bhaumik, M. L., Lacina, W. B., and Mann, M. M., "Exhancement of CO Laser Efficiency by Addition of Xenon," *IEEE Journal of Quantum Electronics*, Vol. QE-6, No. 9, Sept. 1970, pp. 575–576.

[5] Rich, J. W., Thompson, H. M., Treanor, C. E., and Daiber, J. W., "An Electrically Excited Gas-Dynamic Carbon Monoxide Laser," *Applied Physics Letters*, Vol. 19, No. 7, Oct. 1971, pp. 230–232.

[6] Treanor, C. E., Rich, J. W., and Rehm, R. G., "Vibrational Relaxation of Anharmonic Oscillators with Exchange-Dominated Collisions," *Journal of Chemical Physics*, Vol. 48, No. 4, Feb. 1968, pp. 1798–1807.

[7] Bray, K. N. C., "Vibrational Relaxation of Anharmonic Oscillator Molecules: Relaxation Under Isothermal Conditions," *Journal of Physics B (London)*, Ser. 2, Vol. 1, No. 4, July 1968, pp. 705–717; also "II Non-Isothermal Conditions," Vol. 3, No. 11, Nov. 1970, pp. 1515–1538.

[8] McKenzie, R. L., "Vibrational Relaxation and Radiative Gain in Expanding Flows of Anharmonic Oscillators," TR TN-D-7050, March 1971, NASA.

[9] Rich, J. W., "Kinetic Modeling of the High Power CO Laser," *Journal of Applied Physics*, Vol. 42, No. 7, June 1971, pp. 2719–2730.

[10] Center, R. E. and Caledonia, G. E., "Anharmonic Effects in the Vibrational Relaxation of Diatomic Molecules in Expanding Flows," *Applied Optics*, Vol. 10, No. 8, Aug. 1971, pp. 1795–1802; also "Vibrational Distribution Functions in Anharmonic Oscillators," *Journal of Chemical Physics*, Vol. 55, No. 2, July 1971, pp. 552–561.

[11] McKenzie, R. L., "Laser Power at 5 μm from the Supersonic Expansion of Carbon Monoxide," *Applied Physics Letters*, Vol. 17, No. 10, Nov. 1970, pp. 462–464.

[12] Watt, W. S., "Carbon Monoxide Gas Dynamic Laser," *Applied Physics Letters*, Vol. 18, No. 11, June 1971, pp. 487–489.

[13] Gibbs, W. E. K. and McLeary, R., "Uniform Discharges in Flowing CO_2 Laser Mixtures at Atmospheric Pressure," *Physics Letters*, Vol. 37A, No. 3, Nov. 1971, pp. 229–230; also McLeary, R. and Gibbs, W. E. K., "CW CO_2 Laser at Atmospheric Pressure," *IEEE Journal of Quantum Electronics*, Vol. QE-9, No. 8, Aug. 1973, pp. 828–833.

[14] Herzberg, G., *Spectra of Diatomic Molecules*, 2nd ed., Van Nostrand, Princeton, N.J., 1950, p. 129.

[15] Penner, S. S., "Population Temperatures and Translational Temperatures for Free-Radicals in Flames," *Quantitative Molecular Spectroscopy Gas Emissivities*, Addison-Wesley, Reading, Mass., Chap. 17, 1959.

[16] Rich, J. W., Bergman, R. C., Thompson, H. M., and Lordi, J. A., "Electrically Excited Gas Dynamic CO Laser Study," AFAL-TR-73-294, Sept. 1973, U.S. Air Force Avionics Lab., Wright-Patterson Air Force Base, Ohio.

[17] Rich, J. W., Lordi, J. A., and Kang, S. W., "Final Technical Report: Supersonic Electrically Excited Laser Development," Rept. WG-5164-A-3, June 1974, Calspan Corporation, Buffalo, N.Y.

[18] Nighan, W. L., "Electron Kinetic Processes in CO Lasers," AIAA paper 74-563, Palo Alto, Calif., 1974.

[19] Emanuel, G., "RESALE-1: A Chemical Laser Computer Program," Rept. TR-0127 (2776)-1, March 1972, Aerospace Corporation, El Segundo, Calif.